A Galvanic-Isolated Grid-Connected fuel cell single phase AC power generation system with *LCL* filter

Prabhuraj Shanmugham*, Ahmad Ali*, Sakda Somkun*‡

*School of Renewable Energy and Smart Grid Technology, Naresuan University, Phitsanulok, Thailand

(sprabhuraaj@gmail.com, ahmad.nazeri09@gmail.com, sakdaso@nu.ac.th)

‡Corresponding Author; Sakda Somkun, School of Renewable Energy and Smart Grid Technology, Naresuan University, Phitsanulok, Thailand, Tel: +66 852344991, Fax: +66 55963180, sakdaso@nu.ac.th

Received: 27.08.2018 Accepted:25.09.2018

Abstract- Fuel cell system is a promising alternate way of power generation from clean, green fuel such as Hydrogen with almost zero emissions. It can be a primary power or an aiding power to the grid during instability. Grid connected fuel cell systems experience double line frequency ripples from the inverters which affect the life of fuel cells. The current ripples are to be limited within 15% for safe operation of the fuel cells. This paper presents design of a dual active bridge DC-DC converter to step up the low voltage DC output from fuel cell to a high voltage DC with galvanic isolation and a PLL based grid synchronized single phase PWM inverter with *dq* reference frame grid current control suitable for fuel cell systems. Extended Symmetrical Optimum method is used for optimal tuning of the PI controllers. An *LCL* filter is designed for effective ripple attenuation in the grid current with active damping of the resonance in the region of stability. MATLAB/Simulink® is used for the design and is verified with a 1kW Horizon PEM fuel cell system. The power is exported to the grid with measured THD_i of 1.7% in the grid current with reactive power injection by simple phase shift modulation control. The maximum overall system efficiency is measured to be 85%.

Keywords Hydrogen energy, fuel cells, dual active bridge, grid connected inverters, *LCL* filter.

1. Introduction

Green power is an alternate to the fossil power to mitigate the global warming with almost zero GHG emissions [1]. In distributed generation systems, the grid connected renewable energy systems affect the stability of the grid as they are intermittent and fluctuating in nature [2]. In such cases, the hydrogen gas being a green fuel can be used as a storage medium by electrolysis with the excess renewable power from solar PV and wind. The fuel cell power generation systems can aid the grid during instability from the stored hydrogen gas. The fuel cells are highly efficient, less noisy and requires low maintenance with zero emissions [3]. Fuel cells produce low voltage DC power outputs, hence power converters namely DC-DC and DC-AC converters are to be connected for boosting the fuel cell output voltage and to convert the boosted voltage to AC to integrate with grid respectively. These power converters inevitably introduce ripples into the fuel cell systems. The inverters in specific introduce double line frequency ripples into the fuel cell. The current ripples in the fuel cell have to be limited within 15% for safe operation of the fuel cells [4]. The current ripples in addition to affecting the life of the fuel cells, they also affect the consumption of the fuel and the fuel cell capacity [5-6]. These current ripples may result in nuisance tripping due to overload conditions and the fuel cells are overrated around 17% than their nominal power handling requirement to handle such situation [7]. There are various topologies proposed in previous studies [8-12] for DC-DC converters with and without galvanic isolation. A non isolated four phase interleaved boost converter has been investigated for different renewable power applications with a low DC voltage conversion ratio [13]. In a previous study [14], a three phase three level inverter has reported with 2.41% THD_i with a PV system. The grid connected PV inverters has been reported with a maximum efficiency of 97%-98%, which are typically designed for a high DC input range of 350V-750V with single stage conversion from DC to AC [15]. In high power applications and in fuel cell power conversion systems, where the voltage conversion ratio is much higher, non-isolated topologies are to be avoided for safe operation. Among the isolated converters push pull converters and half bridge converters have the problems of identical center tap windings in the transformer and higher

rating of switching devices due to the high stress levels respectively [9].

This paper presents the design of a single phase grid connected fuel cell power generation system consisting of an isolated Dual Active Bridge DC-DC converter and PWM inverter with grid current controlled *LCL* filter under synchronous reference frame control scheme. The section 2 describes the overall system components with control techniques. In section 3, modeling and design of DAB, single phase inverter with *LCL* filter are described. Section 4 presents the design of PI controller for PLL based grid synchronization. To validate the proposed system, the experimental results are reported and discussed in section 5.

2. System Configuration

The dual active bridge (DAB) converter topology is considered in the proposed system for low voltage DC boosting, as it has the desired features like high power density, higher efficiency, and inherent Zero Voltage Switching (ZVS) capability with galvanic isolation [8]. The basic structure of DAB consists of an input bridge, a high frequency transformer with an external leakage inductance and an output bridge as shown in Fig. 1. The input bridge converts the low voltage DC from the fuel cell to a high frequency square wave AC, the high frequency transformer steps up this low voltage AC to a high voltage square wave AC, and the output bridge converts this high voltage AC to high voltage DC. The power transfer through DAB can be easily controlled by simple phase shift modulation technique by controlling the phase difference (ϕ) between the gate signals of the input and output bridges. The power is transferred from the bridge with leading gate signals to the bridge with lagging gate signals. The high frequency transformer, a part of DAB is designed for low load operating voltages where the voltage conversion ratio (d) referred to the primary becomes a function of input voltage (v_{FC}) from the fuel cell which varies dynamically.

The phase shift (ϕ) is modulated according to the required power transfer and the input voltage level (v_{FC}) within the ZVS boundaries for soft switching of the switches to minimize the switching losses [8]. As a preliminary design the DAB is controlled in open loop mode by phase shift modulation.

A single phase unipolar PWM inverter is connected to the DAB to convert the high voltage DC output to an AC signal. An *LCL* filter is designed as the line filter to attenuate the ripples at the grid side. For grid tied inverters *LCL* filters are advantageous over *L* filters due to their higher ripple attenuation factor [16]. The resonance nature of *LCL* filters must be carefully considered during the designing and controlling of the system for stable operation. The line current control is employed which is difficult as it is a time varying signal. If a PI controller in stationary reference frame is used it will be resulting with a finite steady state error. In previous studies, several other stationary frame control techniques such as hysteresis [17], deadbeat [18], predictive [19], repetitive [20] and PR control [21] have been proposed to ensure zero the steady state error. Although the PR controller is becoming more popular due to its simple structure and infinite gain at the desired frequency, it needs a very high gain at resonant frequency to have a small steady state error. This high gain increases the oscillations at the transient time and may lead to instability if the line frequency exceeds the cut off frequency. Hence the design and digital implementation of PR controller becomes more difficult. On the other hand, current control using synchronous reference (dq) frame transforms the time varying physical signals from stationary ($\alpha\beta$) frame to a rotational frame, where the AC components become DC and a standard infinite gain PI controller with zero steady state error can be implemented [22-23]. A Park based PLL is used for grid synchronization to extract the grid parameters such as voltage ($\hat{V}_s$) and frequency (ω_s). An extended SO method [24] is used to find the controller parameters for stable operation of the system. The reduction in grid current ripples reduces the ripples at the fuel cell system. The synchronous reference frame control has enabled the active and reactive power control independently by controlling respective current components $i_d(t)$ and $i_q(t)$. The injection of the reactive power has significantly reduced the grid current ripples.

The proposed galvanic-isolated 1kW single phase grid tied fuel cell power generation system is exhibited in Fig. 1. It consists of a 48 cell 1kW PEM fuel cell, 1kW DAB converter, 1.5kVA single phase PWM inverter with an *LCL* filter. A 99.995% pure hydrogen with a constant pressure of 0.45-0.55 bar is supplied to the system. The no load voltage of the fuel cell system is 45.6V with a maximum power of 1008W at 28.8V, 35A. The fuel cell is connected to DAB to step up its low voltage output to a high voltage which is at least $\sqrt{2}$ times the RMS value of required AC voltage. An input capacitor C_i is connected at the output of the Fuel Cell before the input bridge, which filters the current ripples from being injected into the fuel cell system due to high frequency switching. The gate signals at 20 kHz switching frequency are given to the power switches of the input and output bridges of DAB with a phase shift (ϕ) for required power export from the fuel cell to the grid. This generates a 20 kHz low voltage square wave AC signal at the primary and high voltage square wave AC signal at the secondary of the high frequency transformer. The high voltage square wave AC signal is further converted to a high voltage DC by the output bridge of the DAB. The dynamic nature of the fuel cell is considered in the design of high frequency transformer to give 400 V for the fuel cell voltage of 38V. This 400V high voltage DC is converted to a single phase 230V, 50 Hz AC by an unipolar PWM inverter and synchronized to the grid with Park based PLL. An *LCL* is designed for higher ripple attenuation at the grid side current. An unbalanced *dq* reference frame grid current control which is equivalent to an ideal PR controller [22] is employed with *LCL* filter for zero steady state error.

3. System Design

This section presents the design considerations of 1kW fuel cell power generation system comprising of DAB and PWM inverter with *LCL* filter.

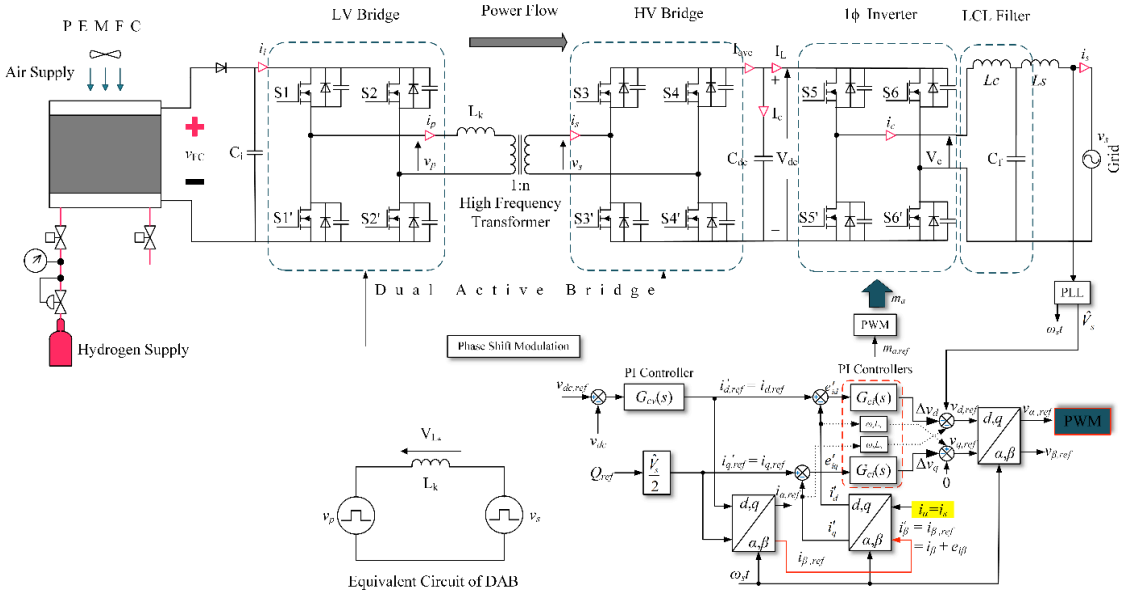

Fig. 1. Fuel cell power generation system.

3.1. Dual Active Bridge

The DAB as depicted in Fig. 1 consists of LV bridge, high frequency transformer and HV bridge for DC voltage boosting. The details of the DAB converter are as given in the Table 1. The voltage and current in the primary and secondary windings of the transformer are as shown in Fig. 2 for the primary referred voltage transfer ratio d<1. The power transfer by the DAB from the fuel cell to the inverter is derived from Fig. 2 and is given by the Eq. (1) [8].

$$P_{FC} = \frac{V_{FC}^2\, d\, \phi}{\pi\, \omega\, L_k}(\pi - \phi) \qquad (1)$$

where V_{FC} is the fuel cell's DC output voltage, ϕ is the phase difference between the bridge switching signals, d is the voltage transfer ratio referred to the primary, L_k is the required leakage inductance of the transformer for power transfer and ω is the switching frequency.

The DAB is designed to handle 1kW power and the switching frequency is considered to be f_{sw}=20kHz. To design the transformer and the leakage inductor the design procedures given in [25] are followed.

3.1.1. Design of high frequency transformer

The dynamic nature of the fuel cell varies its voltage as the current as shown in Fig. 4. This makes the primary referred voltage transfer ratio d as a function of the fuel cell voltage v_{FC} as $d = v'_{dc}/v_{FC}$, where v'_{dc} is the primary referred DAB output voltage. The value of d is taken as 1 at light loads for the design of high frequency transformer so that when the load increases the value of d increases within the limited ZVS boundaries as shown in Fig. 3.

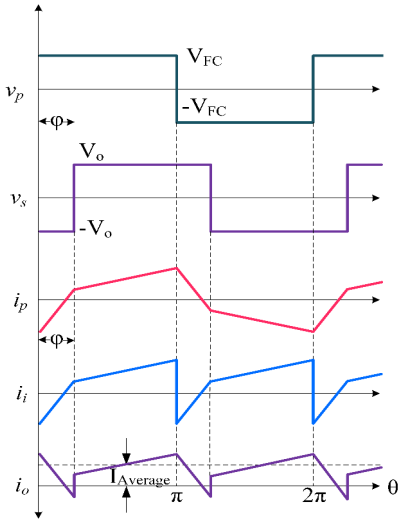

Fig. 2. DAB voltage and current waveforms for d <1.

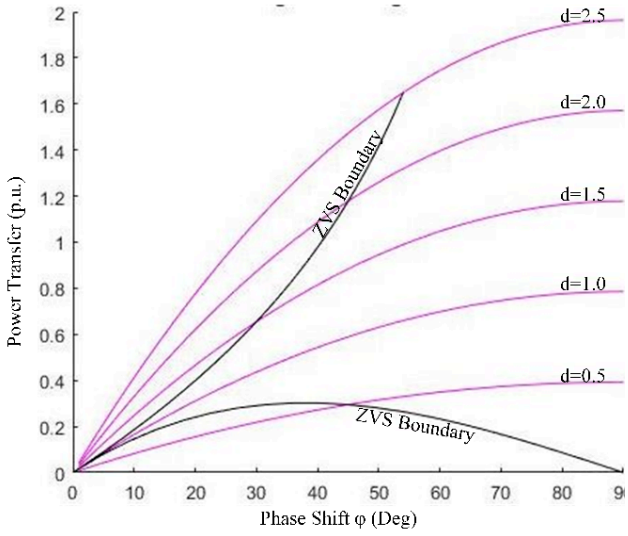

Fig. 3. Zero Voltage Switching boundaries.

Table 1. System Parameters

System	Parameters	Values
Fuel Cell	No. of cells in the PEM fuel cell	48
	No load voltage of fuel cell, v_{FC} (V)	45.6
	Maximum output power from fuel cell (W)	1008
	Maximum power point (V/A)	28.8 / 35
Dual Active Bridge	Power capability (W)	1000
	Switching frequency, f_{sw} (kHz)	20
	Transformer turns ratio 1:n	1:10.6
	Leakage inductance, L_k (mH)	89
	DC link voltage, V_{dc} (V)	400
	DC link capacitance, C_{dc} (µF)	1100
Single phase inverter	RMS Line voltage, v_s (V)	230
	Line frequency, f_s (Hz)	50
	Switching frequency, f_{swi} (kHz)	10
	Apparent power, S_n (kVA)	1.5
	PWM technique	Unipolar
LCL filter	Grid side inductance, L_s (mH)	0.35
	Inverter side inductance, L_c (mH)	3.4
	Filter capacitance, C_f (µF)	2.25
	Resonance frequency, f_r (kHz)	6
PI controller – current loop	Proportional gain, K_{pi}	0.793
	Integral gain, K_{ii}	0.0991
PI controller – voltage loop	Proportional gain, K_{pv}	11.6238
	Integral gain, K_{iv}	0.0978

In this design the d=1 is considered at the fuel cell voltage of v_{FC} =38V. Hence the value of d typically varies from 1-1.26 for the voltage (v_{FC}) variation of 38V-30V. The output voltage of the transformer is considered as 400V which is needed for the further AC conversion by the inverter, which gives the turns ratio as 1:10.6 at d=1. The primary RMS current of 40.2A is taken from the MATLAB simulation results for the design which results with 3.82 A as the secondary current for the given turns ratio. An *N87* is considered as magnetic core material with a maximum allowable flux density of 180mT to avoid the saturation. The core geometry of two *E65* cores has met the electrical design specifications of the transformer, hence two *E65* cores are stacked together to construct the transformer. The primary of the transformer is wound with 5 turns of 5 x AWG 12 served *Litz* wires. The secondary of the transformer is wound with 53 turns of 2 x AWG 20 served *Litz* wires. *Litz* wires are used to minimize the losses due to skin effect and the primary and secondary winding terminals are properly terminated.

3.1.2. Design of leakage inductor

The value of leakage inductance L_k is calculated for the maximum power transfer with the maximum allowable phase shift for ZVS operation in the range of d. The leakage inductor is designed for the secondary side connection of the transformer due to low current handling requirement. The value of the leakage inductance is calculated as 89mH for a voltage of 420V, phase shift of 60˚ and a maximum power of 1100W. A little higher voltage (5%) and power (10%) are considered in the design for safety reasons. An *N87* material is chosen for the core and an allowable flux density of 290mT is considered for the design to avoid the magnetic saturation. The core geometry of *ETD49* core has met the electrical design specifications of the required leakage inductor. Hence the inductor is constructed with 118 turns of served *Litz* wires of 2 x AWG 20 on *ETD49* core.

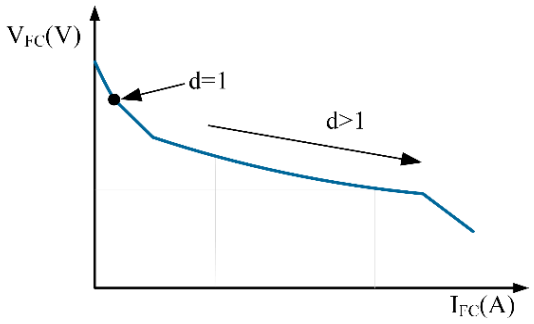

Fig. 4. Fuel cell polarization curve with *'d'* variation [3]

3.2. Single Phase Inverter

A single phase grid synchronized PWM inverter is designed to convert the DC output of the DAB to an AC as shown in Fig. 1. An *LCL* filter is designed as the line filter to reduce the ripples with higher attenuation. An unbalanced *dq* reference frame current control is employed with an *LCL* filter for zero steady state error. The inverter system in physical axis [22] is represented as given by the Eq. 2(a) - Eq. 2(d).

$$C_{dc}\frac{dv_{dc}(t)}{dt} = i_o(t) - m_a(t).i_c(t) \quad (2(a))$$

$$L_c\frac{di_c(t)}{dt} + R_c.i_c(t) = m_a(t).v_{dc}(t) - v_{cf}(t) \quad (2(b))$$

$$C_f\frac{dv_{cf}(t)}{dt} = i_c(t) - i_s(t) \quad (2(c))$$

$$L_s\frac{di_s(t)}{dt} + R_s.i_s(t) = v_{cf}(t) - v_s(t) \quad (2(d))$$

where $m_a(t)$ is the modulating signal, C_{dc} and v_{dc} are the DC link capacitor and its voltage, $i_o(t)$,$i_c(t)$ and $i_s(t)$ are the output dc current from DAB, inverter and grid side currents respectively. L_c, R_c and L_s, R_s are the inverter and grid side inductances with their respective winding resistances (R_c and R_s are not shown in Fig. 1 for simplicity). The voltage across the filter capacitor C_f is denoted by v_{cf}.

The inverter system can be represented in *dq* reference frame by applying Park's transformation in *dq* axis as shown in Fig. 1 and inverse Park's transformation to get $i_\alpha(t)$. The β axis current $i_\beta(t)$ is obtained by phase delaying the measured line current $i_\alpha(t)$ by $\pi/2$. The value of real power transfer and reactive power injection decides the value of reference currents $i_{d,ref}(t)$ and $i_{q,ref}(t)$ of the control circuit respectively. The line voltage magnitude and phase angle $\omega_s t$ are extracted using Park based PLL from the line to generate reference signal $v_{\alpha,ref}$ for grid synchronization. An unipolar PWM signals are generated at f_{swi}=10 kHz to have the equivalent switching frequency of 20 kHz. The unipolar PWM has lower harmonics and the power switches experience half the voltage stress than the bipolar PWM.

3.3. LCL Filter

The *LCL* filters have higher ripple attenuation factor than *L* filters which makes them more suitable for grid connected inverters [26]. The stability of system with *LCL* filters is affected due to their inherent resonance nature. The *LCL* filter should be carefully designed and controlled for stable operation of the system. The transfer function of *LCL* filter for grid current to inverter side voltage is as given in Eq. (3).

$$\frac{i_s}{v_c} = \frac{1}{s^3 L_c L_s C_f + s(L_c + L_s)} \quad (3)$$

$$\frac{i_s}{v_c} = \frac{1}{sL} \quad (4)$$

To design the *LCL* filter, it is approximated as *L* ($=L_c+L_s$) filter as in Eq. (4) by neglecting the filter capacitance C_f as it behaves similar to *L* filter till resonance frequency. The Bode plot of *LCL* filter is shown in Fig. 5. The design of *LCL* filter depends on the required level of ripple attenuation, switching frequency, applied PWM technique and the reactive power requirement [27]. The inverter system design specifications are as listed in Table 1. The *LCL* system parameters are calculated [26] by choosing the switching frequency f_{swi} as 10 kHz, the resonance frequency f_r as 6 kHz within the stability region [28], the maximum allowable current ripples at inverter side as 16% and the percentage of reactive power absorption as 2.5%. The values of inverter side inductance L_c, grid side inductance L_s and filter capacitance C_f are as listed in the Table 1. The inductance in total must be < 0.1 p.u to reduce the AC voltage drop in the inductors [27]

To construct the inductors, proper magnetic core, wire size and number of turns are chosen as per calculated values of inductors L_c and L_s. The current factor k_i, window utilization factor k_u and temperature rise ΔT are chosen accordingly. The area product A_p of the required cores for L_c and L_s helps in the selection of the core sizes. The maximum

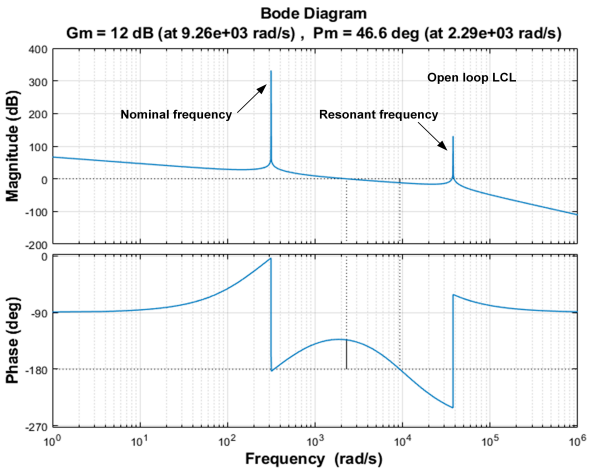

Fig. 5. Bode diagram *LCL* filter.

flux density B_{max} is considered within the saturation flux density B_{sat} of the core material and is selected to be 0.35 T [29]. The converter side inductor L_c was constructed from a *T300-26* iron powder core stacked together with a *T300-26D*, with 120 turns of a 1.9mm diameter enameled copper wire. The grid side inductor L_s was wound with 46 turns using enameled copper wire of 1.7 mm diameter on a *T184-26* iron powder core.

4. Design of PI Controller

An extended Symmetrical Optimum (SO) method [24] is used to find the PI controller parameters for grid side current control. The approximated *LCL* filter as *L* filter by neglecting C_f ease the design of PI controller. In digital control systems, time delay is inevitable which affects the system behaviour resulting to an unstable system [30]. Hence a first order time delay is introduced with a delay time $T_d = T_s + T_{PWM} = 1.5T_s$ to compensate the sampling and computational time delays for digital PWM implementation. The grid current control loop is as shown in Fig. 6. The transfer function of *LCL* filter in open loop after *L* approximation is as given in Eq. 5.

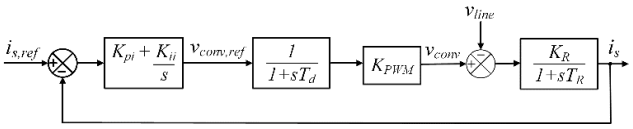

Fig. 6. Grid side current control loop in *dq* frame.

$$G_{OL,i} = \left(K_{pi} + \frac{K_{ii}}{s}\right)\cdot\left(\frac{1}{1+sT_d}\right)\cdot\left(\frac{K_R}{1+sT_R}\right) \quad (5)$$

where $T_s=1/f_{sw}$, $R=R_c+R_s$, $T_R=L/R$, and $K_R=V_{dc}/R$.

The *LCL* filter transfer function in closed loop is given by

$$G_{CL,i} = \frac{K_{pi}K_R s + K_{ii}K_R}{T_R T_d s^3 + T_R s^2 + K_{pi}K_R s + K_{ii}K_R} \quad (6)$$

The extended symmetrical optimum method yields the PI controller parameters as $K_{pi} = \frac{T_R}{2K_R T_d}$ and $K_{ii} = \frac{T_R}{8K_R T_d^2}$.

The DC link voltage control loop for single-phase grid-connected VSCs is depicted in Fig. 7. A first order LPF is added in series with the PI controller of the voltage control loop. The PI controller is tuned by the extended SO method in selecting the LF time constant T_f as well as the PI controller parameters. The voltage ripples in DC bus are mainly due to the grid oscillating power $\tilde{p}_s(t)$. The LPF helps in attenuating the ripple power further down to -40 dB/decade. A bandwidth of 10 Hz is selected for the DC link voltage control loop to reduce the 100 Hz ripple components in the DC link voltage, while the high bandwidth of the line current loop ($G_{CL,i}$) is approximated to be with unity gain.

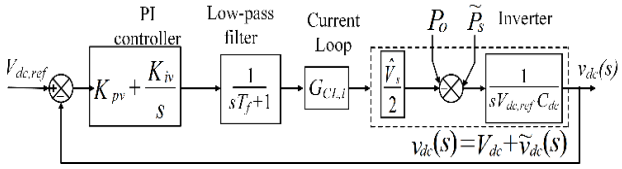

Fig. 7. DC link voltage control loop.

5. Experimental Results and Discussion

The 1 kW PEM fuel cell power generation system was designed as per the design specifications suitable to the Horizon H-1000 fuel cell. The DC link capacitor was initially charged to 400V with the help of grid connected converter to avoid the inrush current at the starting of fuel cell system. The required control signals were generated by TMS320F28069 Piccolo microcontroller. The LV bridge of DAB was given with leading gate signals whereas HV bridge with lagging signals to enable the power export from the input LV bridge to the output HV bridge. The phase angle ϕ between the gate signals was adjusted to limit the power transfer from the fuel cell to the grid. The transients in voltage and current of the fuel cell at 650W load is shown in Fig. 8 which also depicts the typical phenomenon called "charge double layer effect".

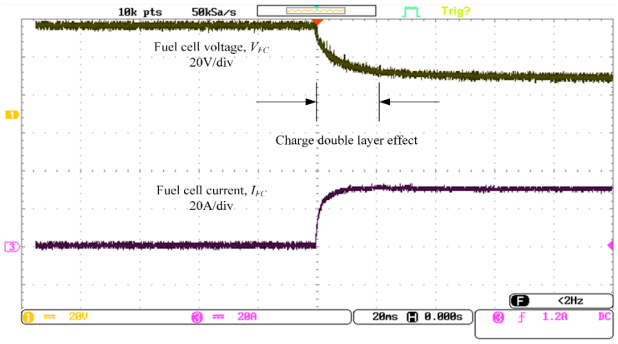

Fig. 8. Fuel cell voltage and current transients at 650W

The voltage and current waveforms measured in the primary and secondary of the transformer are shown in Fig. 9 at $\phi = 60°$ phase shift. The soft switching of the switches in the DAB is achieved as per the ZVS boundary conditions [8], where the currents in the transformer $i_p(\theta)<0$ at the time of LV bridge switching and $i_s(\theta)>0$ at the time of HV bridge switching which ensures the ZVS as shown in Fig. 9. As the power transfer was increased the input voltage from the fuel cell reduced below 38V to increase the power in accordance with the fuel cell polarization curve. Hence the dual active bridge operated in boost mode where the primary referred voltage transfer ratio d >1 as described in Fig. 4 and the voltage loop of the inverter regulated the DC bus at 400V.The measured gird side voltage and current at 650W power export with a phase shift of $\phi = 60°$ are shown in Fig. 10.

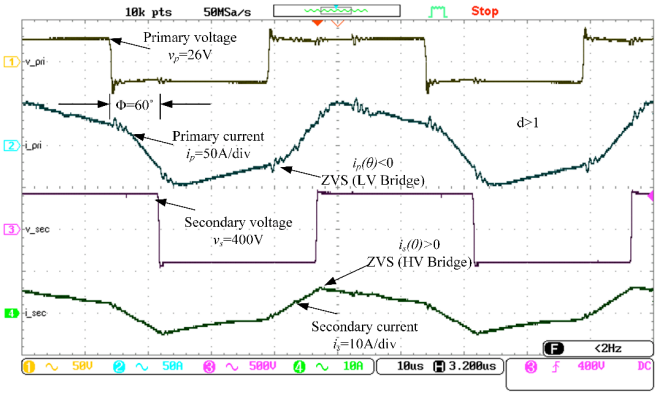

Fig. 9. DAB voltage and current waveforms with ϕ=60˚

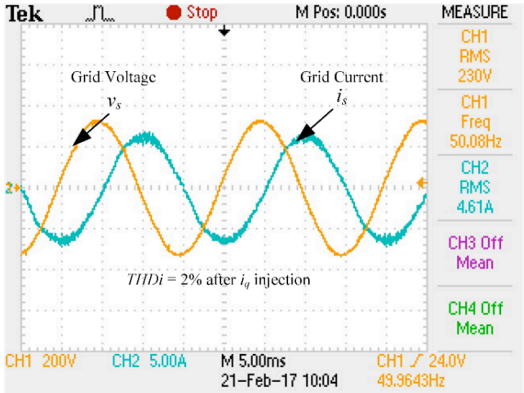

Figure 10. Grid side voltage and current at 650W power with reactive power injection.

The grid side current was measured with more ripples with THD_i of 5% without the injection of q-axis current. When the q-axis current was injected the grid side current THD_i got reduced from 5% to 1.7% for the same 650W power transfer [31]. The reduced current ripples at the grid side current reduces the ripples at fuel cell system which in turn extends their life. The FFT of the fuel cell current at 650W power export is shown in Fig. 11 which ensures the current ripples are less than 1% which is well below the standards [4]. Table 2 gives the comparison between the proposed system and commercially available products [32-34]. The maximum efficiency of the proposed DAB and inverter system is measured as 85 % and the system was stable for entire power transfer range. The efficiency is little lower as it's a two stage conversion as the DC conversion ratio is quite high nearly 10.6.

Table 2. Comparison of proposed system with commercial products

Brand	Rated power	Rated DC input voltage (V)	Peak efficiency (%)	Grid current *THDi* (%)
ABB	1.2 kVA	185	94.8	< 3:5
Schneider	2.8 kW	195 - 550	95.2	< 3
Leonics	1.5 kW	200 - 420	94.3	< 4
Proposed System	1 kW	30 - 38	85	< 2

The measured overall system efficiency and grid side THD_i for various phase shifts are shown in Fig. 12 and Fig. 13 respectively. The efficiency and grid current THD_i are found to be higher at light loads without the injection of $i_q(t)$. At higher loads the efficiency of the system remains the same but the THD_i gets reduced to 1.7 % with the injection of $i_q(t)$. The power exported to the grid and the grid current THD_i were measured using a leakage clamp meter METREL-MD9272.

In order to increase the inverter efficiency hybrid modulation can be employed, but the switching ripple in current is equal to 1 x switching frequency, which results with higher filtering requirements, whereas the unipolar PWM which is used, gives the switching ripple in current as 2 x switching frequency, which lowered the filtering requirements [35]. Moreover in the traditional single phase shift modulation technique, only the average power transfer is managed and other factors such as circulating reactive power, current in transformer are not considered. This results in higher converter loss, greater current stress and hence reduced performance of the DAB. However, the dual phase shift modulation and triple phase shift modulation techniques increase the DAB conversion efficiency by eliminating the circulating reactive power and reducing the current stress [36-38]. In addition to control techniques, the system efficiency can also be increased with the use of SiC power devices and nanocrystalline soft magnetic cores, but at the cost of higher price. Features such as wider bandgap, high-breakdown voltage, high-operating temperature, high-switching frequency and low losses will improve the efficiency with SiC devices [39]. Similarly smaller volume, lower weight, lesser copper losses, extended temperature range, larger safety margins of nanocrystalline soft magnetic cores result in highly efficient robust system [40-41].

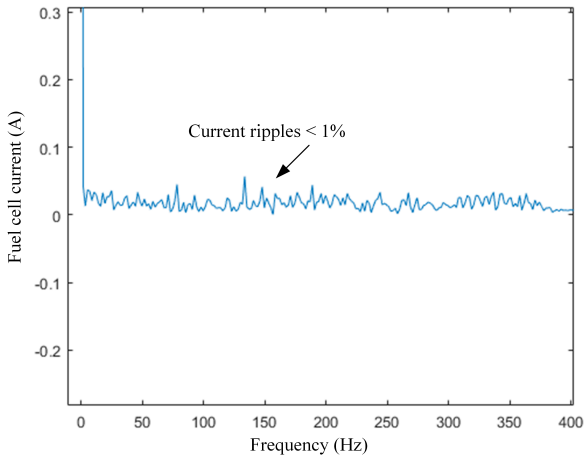

Fig. 11. FFT of Fuel cell current at 650W load

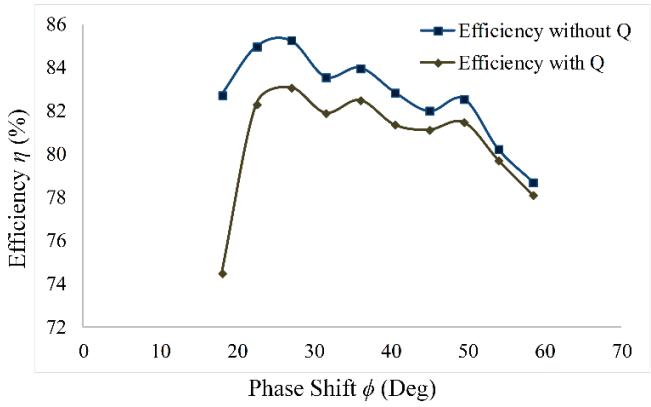

Fig. 12. System efficiency for various phase shifts

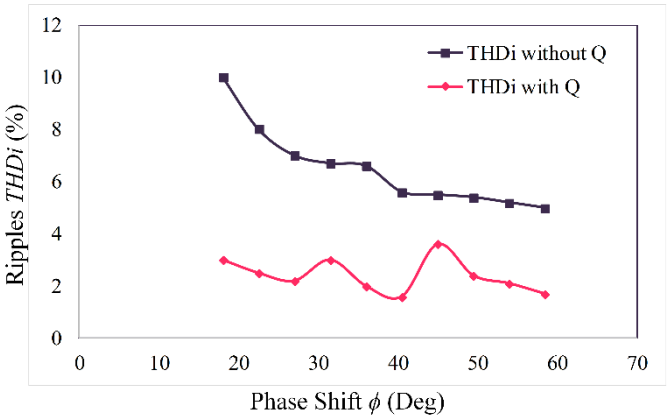

Fig. 13. Grid current THD_i for various phase shifts

The experimental setup of the grid connected 1kW fuel cell power generation system is shown in Fig. 14.

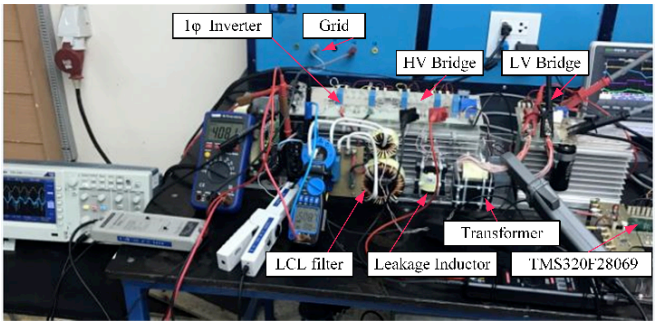

Fig. 14. Experimental setup

6. Conclusion

The experimental results have shown that the dual active bridge DC-DC converters are well suited for grid connected fuel cell systems, with fuel cell current ripples <1%, which enables the safe power transfer with simple phase shift modulation technique with galvanic isolation. The high frequency switching operation made the system very compact with reduced size of passive and magnetic components. The inherent soft switching nature of DAB reduces the switching losses in the system resulting with multistage conversion efficiency of 85% with higher DC conversion ratio 1:10.6. The independent, unbalanced synchronous reference frame current control on grid side current with *LCL* filter is found to be more effective in ripple reduction with *THDi* as low as 1.7% by reactive power injection. The use of *LCL* filter has significantly reduced the ripples at the grid side due to its higher ripple attenuation nature. A careful design of *LCL* filter and symmetrical optimum tuned PI controller made the system stable over the operating range of the system. At higher loads the efficiency of the system remained the same with and without reactive power injection but the THD_i in the grid side current got reduced with reactive power injection. Hence these single phase fuel cell power systems can support the grid on stability from the stored hydrogen energy in the fast growing distributed power generation systems where grid connected renewable systems make the grid unstable due to intermittent nature of the resources.

Acknowledgements

This work was financially supported by the National Research Council of Thailand (project entitled “Development of Alternative Energy Prototypes for Green Communities”).

References

[1] International Energy Agency, "World energy outlook 2016 : Executive summary" IEA, Paris Cedex France, 2016, Available: http://www.iea.org , Last visited : August 05, 2018.

[2] Winter, C.J., "Hydrogen energy - abundant, efficient, clean: A debate over the energy-system-of-change", International Journal of Hydrogen Energy, vol.34, pp.S1-S52, 2009.

[3] James, L. and D. Andrew, Fuel cell systems explained, 2nd ed., John Wiley & Sons Ltd, 2003, pp. 22-23.

[4] EG & G Technical Services Inc., Fuel cell handbook, 7th ed., U.S. Department of Energy, 2004, pp.8.43-8.44.

[5] Choi, W., P.N. Enjeti, and J.W. Howze, "Development of an equivalent circuit model of a fuel cell to evaluate the effects of inverter ripple current", Applied Power Electronics Conference and Exposition, Anaheim, pp.355-361, 2004.

[6] Fontes, G., C. Turpin, S. Astier, and T.A.Meynard, "Interactions between fuel cells and power converters: Influence of current harmonics on a fuel cell stack", IEEE Transactions on Power Electronics, vol.22, pp.670-678, 2007.

[7] Liu, C. and J.S. Lai, "Low frequency current ripple reduction technique with active control in a fuel cepower system with inverter load", IEEE Transactions on Power Electronics, vol.22, pp.1429-1436, 2007.

[8] De Doncker, R.W.A.A., D.M. Divan, and M.H. Kheraluwala, "A three-phase soft-switched high-power-density DC/DC converter for high-power applications", IEEE Transactions on Industry Applications, vol.27, pp.63-73, 1991.

[9] Kirubakaran, A., S. Jain, and R.K. Nema, "A review on fuel cell technologies and power electronic interface", Renewable and Sustainable Energy Reviews, vol.13, pp.2430-2440, 2009.

[10] Nan, C. and R. Ayyanar, "Dual active bridge converter with PWM control for solid state transformer application", IEEE Energy Conversion Congress and Exposition 2013, Denver, pp.4747-4753, 2013.

[11] Ngo, T., J. Won, and K. Nam, "A single-phase bidirectional dual active half-bridge converter”, Applied Power Electronics Conference and Exposition, Orlando, pp.1127-1133, 2012.

[12] Tao, H., A. Kotsopoulos, J.L. Duarte, and M.A.M. Hendrix, "Transformer-coupled multiport ZVS bidirectional DC-DC converter with wide input range", IEEE Transactions on Power Electronics, vol.23, pp.771-781, 2008.

[13] RAMASAMY S, Abishri P, and Umashankar S. “Review of coupled two and three phase interleaved boost converter (IBC) and investigation of four phase IBC for renewable application”, International Journal of Renewable Energy Research (IJRER), vol. 6, pp.421-34, 2016.

[14] Melicio R, Fialho L, Mendes V, and Estanqueiro A. “Simulation of a-Si pv system grid connected by boost and inverter”, International Journal of Renewable Energy Research (IJRER), vol. 5, pp.443-51, 2015.

[15] Blaabjerg F, and Koutroulis E. “Methods for the optimal design of grid-connected PV inverters”, International Journal of Renewable Energy Research (IJRER), vol. 1, pp.54-64, 2011.

[16] Blaabjerg, F., R. Teodorescu, M. Liserre, and A.V. Timbus, "Overview of control and grid synchronization for distributed power generation systems", IEEE

Transactions on Industrial Electronics, vol.53, pp.1398-1409, 2006.

[17] S. K. Khadem, M. Basu, and M. F. Conlon, "Harmonic power compensation capacity of shunt active power filter and its relationship with design parameters", IET Power Electron., vol. 7, pp. 418-430, 2014.

[18] P. Mattavelli, "An improved deadbeat control for UPS using disturbance observers", IEEE Trans. Ind. Electron., vol. 52, pp. 206-212, 2005.

[19] Y. Chen, A. Luo, Z. Shuai, and S. Xie, "Robust predictive dual-loop control strategy with reactive power compensation for single-phase grid-connected distributed generation system", IET Power Electron., vol. 6, pp. 1320-1328, 2013.

[20] S. Dasgupta, S. K. Sahoo, and S. K. Panda, "Single-phase inverter control techniques for interfacing renewable energy sources with microgrid-part I: parallel-connected inverter topology with active and reactive power flow control along with grid current shaping", IEEE Trans. Power Electron., vol. 26, pp. 717-731, 2011.

[21] M. C. Kisacikoglu, M. Kesler, and L. M. Tolbert, "Single-phase on-board bidirectional PEV charger for V2G reactive power operation", IEEE Trans. Smart Grid, vol. 6, pp. 767-775, 2015.

[22] Somkun, S. and V. Chunkag, "Unified unbalanced synchronous reference frame current control for single-phase grid-connected voltage-source converters", IEEE Transactions on Industrial Electronics, vol.63, pp.5425-5436, 2016.

[23] Miranda, U.A., L.G.B. Rolim, and M. Aredes, "A dq synchronous reference frame current control for single-phase converters", Power Electronics Specialists Conference, Recife, pp.1377-1381, 2005.

[24] Preitl, S. and R.E. Precup, "An extension of tuning relations after symmetrical optimum method for PI and PID controllers", Automatica, vol.35, pp.1731-1736, 1999.

[25] Erickson, R.W. and D. Maksimović, Fundamentals of power electronics, 2nd ed., Kluwer Academic Publishers, 2001, pp. 565-583.

[26] Ahmad, A., S. Prabhuraj, and S. Sakda, "Single-phase grid-connected voltage source converter for LCL filter with grid-current feedback", 5th International Electrical Engineering Congress, Pattaya, pp. 1-6, 2017.

[27] Liserre, M., F. Blaabjerg, and S. Hansen, "Design and control of an LCL-filter-based three-phase active rectifier", IEEE Transactions on Industry Applications, vol.41, pp.1281-1291, 2005.

[28] Dannehl, J., C. Wessels, and F.W. Fuchs, "Limitations of voltage-oriented PI current control of grid-connected PWM rectifiers with LCL filters", IEEE Transactions on Industrial Electronics, vol.56, pp.380-388, 2009.

[29] Hurley, W.G. and W.H. Wölfle, Transformers and inductors for power electronics: Theory, design and applications, 1st ed., John Wiley & Sons Ltd, 2013, pp. 55-74.

[30] Zou, C., B. Liu, S. Duan, and R. Li, "Influence of delay on system stability and delay optimization of grid-connected inverters with LCL filter", IEEE Transactions on Industrial Informatics, vol.10, pp.1775-1784, 2014.

[31] Zong, X. and P.W. Lehn, "Reactive power control of single phase grid tied voltage sourced inverters for residential PV application", Annual Conference of IEEE Industrial Electronics, Montreal, pp.696-701, 2012.

[32] ABB string inverters. Available from: http://new.abb.com/power-convertersinverters/solar/string/single-phase/uno-dm-1-2kw-2-0kw-3-3kw-4-0kw-4-6kw-5-0kwtl-plus, Last visited : September 22, 2018

[33] Single phase grid-tie solar inverter. Available from: https://www.schneiderelectric.com/en/product/878-2801/conext---single-phase-grid-tie-solar-inverter-tx-2800-na---2800-w-output/, Last visited : September 22, 2018

[34] Grid connected inverter with isolation transformer. Available from: http://www.leonics.com/product/renewable/inverter/dl/G-4000-176.pdf, Last visited : September 22, 2018.

[35] Teodorescu R, Liserre M, Rodriguez P. Grid converters for photovoltaic and wind power systems. vol. 29. John Wiley & Sons; 2011, pp. 9-11.

[36] Kim, Myoungho, Martin Rosekeit, Seung-Ki Sul, and Rik WAA De Doncker. "A dual-phase-shift control strategy for dual-active-bridge DC-DC converter in wide voltage range." In Power Electronics and ECCE Asia (ICPE & ECCE), 2011 IEEE 8th International Conference on, pp. 364-371. IEEE, 2011.

[37] Feng, Bo, Yubin Wang, and Jingbin Man. "A novel dual-phase-shift control strategy for dual-active-bridge DC-DC converter." In Industrial Electronics Society, IECON 2014-40th Annual Conference of the IEEE, pp. 4140-4145. IEEE, 2014.

[38] Wen, H., and W. Xiao. "Bidirectional dual-active-bridge dc-dc converter with triple-phase-shift control." In Applied Power Electronics Conference and Exposition (APEC), 2013 Twenty-Eighth Annual IEEE, pp. 1972-1978. IEEE, 2013.

[39] Biela, J., M. Schweizer, S. Waffler, and J. W. Kolar. "SiC vs. Si-evaluation of potentials for performance improvement of inverter and DC-DC converter systems by SiC power semiconductors." IEEE transactions on industrial electronics, vol. 58, pp. 2872-2882, 2011.

[40] She, Xu, Alex Q. Huang, and Rolando Burgos. "Review of solid-state transformer technologies and their application in power distribution systems." IEEE Journal of Emerging and Selected Topics in Power Electronics, vol. 1, pp. 186-198, 2013.

[41] Rylko, Marek S., Kevin J. Hartnett, John G. Hayes, and Michael G. Egan. "Magnetic material selection for high power high frequency inductors in dc-dc converters." In Applied Power Electronics Conference and Exposition, 2009. APEC 2009. Twenty-Fourth Annual IEEE, pp. 2043-2049. IEEE, 2009.